The Bismuth Abundance in the HGMN Stars chi Lupi and HR 7775 and Improved Atomic Data for Selected Transitions of BI I, BI II, and BI III

Wahlgren, Glenn; Brage, Tomas; Brandt, J. C.; Fleming, J.; Johansson, Sveneric; Leckrone, D. S.; Proffitt, C. R.; Reader, J.; Sansonetti, C. J.

Published in:
Astrophysical Journal

DOI:
10.1086/320063

2001

THE ASTROPHYSICAL JOURNAL, 551:520–535, 2001 April 10

THE BISMUTH ABUNDANCE IN THE HgMn STARS χ LUPI AND HR 7775 AND IMPROVED ATOMIC DATA FOR SELECTED TRANSITIONS OF Bi I, Bi II, AND Bi III[1]

G. M. WAHLGREN,[2,3] T. BRAGE,[2] J. C. BRANDT,[4] J. FLEMING,[5] S. JOHANSSON,[2,6] D. S. LECKRONE,[7] C. R. PROFFITT,[8,9] J. READER,[10] AND C. J. SANSONETTI[10]

Received 2000 May 25; accepted 2000 December 11

ABSTRACT

High-resolution spectra of the chemically peculiar HgMn stars χ Lupi and HR 7775, obtained with the *Hubble Space Telescope*/Goddard High Resolution Spectrograph, are investigated for their abundance of bismuth by comparison with LTE synthetic spectrum modeling. HR 7775, previously known from *International Ultraviolet Explorer* spectra to display strong lines of Bi II, is determined to have bismuth present at an enhancement level of nearly 5 orders of magnitude from the lines Bi II λλ1436, 1902 and Bi III λ1423. The bismuth enhancement for χ Lupi is found to be near a level of 1.5 dex, and an ionization anomaly between Bi^+ and Bi^{++} is apparent. HR 7775 abundance enhancements of the heavy elements platinum, [Pt/H] = 4.7 dex, and gold, [Au/H] = 3.8 dex, have also been determined. New laboratory measurements for wavelengths and hyperfine structure patterns of Bi I/Bi II/Bi III lines are presented, as well as the results of calculations for hyperfine structure constants and oscillator strengths for selected lines of Bi II and Bi III.

Subject headings: atomic data — stars: abundances — stars: chemically peculiar — stars: individual (χ Lupi, HR 7775) — ultraviolet: stars

On-line material: machine-readable tables

1. INTRODUCTION

The chemically peculiar (CP) stars of the upper main sequence are renowned for displaying anomalous spectral line strengths for a variety of elements. Of particular note are the enhanced strengths of the rare earth elements in the spectra of the magnetic A-type stars and the very heavy elements Pt, Au, Hg, and Tl in the spectra of the non-magnetic, late B, HgMn stars. While radiative diffusion theory (Michaud 1970) has provided a basic framework for study into the origins of anomalous line strengths, additional work must be undertaken to account for the diversity of elemental abundance and isotopic mixture anomalies that are observed in HgMn stars. Recent theoretical work by Seaton (1997, 1999) has addressed the behavior of iron group elements in unevolving models. Other modeling efforts (Proffitt et al. 1999; Leckrone et al. 1996) have been unable to maintain the great line enhancements over extended periods of time. Thus, temporal evolution may enter into the problem in presently unknown ways.

χ Lupi (=HD 141556, B9.5p HgMn+A2Vm) has been the subject of extensive study at visible and ultraviolet wavelengths. As part of the χ Lupi Pathfinder Project (Leckrone et al. 1998, 1999) the ultraviolet high spectral resolution capabilities available on the *Hubble Space Telescope* (*HST*) have been exploited. The project goals have included the study of elemental abundances and isotopic mixtures in the atmosphere of one HgMn star in order to provide constraints for the diffusion paradigm or any other theory that proposes to explain the spectral anomalies of late B-type chemically peculiar stars. The choice of χ Lupi for such a target is predicated upon its extremely sharp-lined spectrum and the anomalous isotopic composition observed at optical wavelengths for the heavy elements platinum and mercury. Its brightness (m_v = 3.95) has also allowed for rather high signal-to-noise ratio (S/N) levels to be attained with reasonable exposure durations using the Goddard High Resolution Spectrograph (GHRS) on board *HST*.

HR 7775 (=HD 193452, B9.5p HgMn) represents a logical next step in the overall process of testing the diffusion paradigm since its effective temperature is essentially identical to that of χ Lupi A, and the spectra of these two stars are similar overall. HR 7775 also displays extremely narrow spectral lines, indicative of low rotational velocity and small atmospheric turbulence. Its surface gravity is, however, slightly greater than that of χ Lupi A. This may indicate a somewhat less advanced stage of evolution for HR 7775, but the singular trait that has brought attention to HR 7775 is the great enhancement of bismuth lines in its spectrum. Using ultraviolet spectra obtained with the *International Ultraviolet Explorer* (*IUE*) satellite, Jacobs &

[1] Based on observations with the NASA/ESA *Hubble Space Telescope*, obtained at the Space Telescope Science Institute, which is operated by the Association of Universities for Research in Astronomy, Inc., under NASA contract NAS5-26555.

[2] Department of Physics, University of Lund, Box 118, 221 00 Lund, Sweden; Glenn.Wahlgren@fysik.lu.se, Tomas.Brage@fysik.lu.se, Sveneric.Johansson@fysik.lu.se.

[3] Science Programs, Computer Sciences Corporation, Code 681, Goddard Space Flight Center, Greenbelt, MD 20771.

[4] Laboratory for Astronomy and Space Physics, University of Colorado, Boulder, CO 80309; brandt@lyrae.colorado.edu.

[5] Department of Applied Mathematics, Queen's University of Belfast, Belfast, BT7 1NN, Northern Ireland.

[6] Lund Observatory, Lund University, Box 43, 221 00 Lund, Sweden.

[7] *Hubble Space Telescope* Project, NASA Goddard Space Flight Center, Code 440, Greenbelt, MD 20771; dleckrone@hst.nasa.gov.

[8] Science Programs, Computer Sciences Corporation, 3700 San Martin Drive, Baltimore, MD 21218; proffitt@stsci.edu.

[9] Department of Physics, Institute for Astrophysics and Computational Sciences, The Catholic University of America, 200 Hannan Hall, Washington, DC 20064.

[10] National Institute of Standards and Technology, Gaithersburg, MD 20899; joseph.reader@nist.gov, craig.sansonetti@nist.gov.

TABLE 1

WAVELENGTHS FOR Bi I

λ_{vac}[a] (Å)	Int.	σ (cm^{-1})	Odd Level[b] (cm^{-1})	J_{odd}	Even Level[b] (cm^{-1})	J_{even}	λ_{calc}[c] (Å)	Comment[d]
1685.698.....	70	59322.61	...	...	...	...	...	...
1687.055.....	50	59274.89	...	...	...	...	...	...
1716.049.....	30	58273.39	0	3/2	58273[e]	3/2[f]	...	...
1731.050.....	3	57768.41	0	3/2	57767[e]	3/2	...	...
1735.928.....	25	57606.08	0	3/2	57607[e]	1/2	...	...
1743.760.....	50	57347.34	...	...	...	...	...	...
1752.065.....	5000	57075.51	0	3/2	57075	5/2	1752.0757(15)	...
1756.414.....	20	56934.19	0	3/2	56934	5/2	1756.4145(2)	...
1757.587.....	75	56896.19	0	3/2	56896	3/2	1757.5879(16)	...
1767.023.....	1	56592.36	0	3/2	56591[e]	1/2	...	...
1767.737.....	9000	56569.50	0	3/2	56569	3/2	1767.7383(16)	...
1775.254.....	10	56329.97	0	3/2	56329	3/2	1775.2538(2)	...
1788.606.....	2	55909.46	11419	3/2	67327[g]	?	...	...
1791.328.....	20	55824.51	0	3/2	55824	1/2	1791.3273(2)	...
1802.626.....	300	55474.62	0	3/2	55474	5/2	1802.6231(2)	...
1804.233.....	20	55425.21	0	3/2	55425	3/2	1804.2302(2)	...
1832.824.....	300	54560.61	0	3/2	54560	1/2	1832.8232(2)	...
1849.498.....	20	54068.73	11419	3/2	65483[e]	3/2	...	...
1852.638.....	2000	53977.09	0	3/2	53977	5/2	1852.6392(2)	...
1856.017.....	350	53878.82	0	3/2	53878	3/2	1856.0165(2)	...
1913.666.....	1500	52255.72	0	3/2	52255	1/2	1913.6662(3)	...
1954.706.....	15000	51158.59	0	3/2	51158	5/2	1954.7096(3)	...
1960.049.....	6000	51019.13	0	3/2	51019	3/2	1960.0506(3)	...
2021.801.....	4000	49460.85	0	3/2	49460	3/2	2021.7986(3)	Flag; −0.06; 2021.772
2062.293.....	150000	48489.72	0	3/2	48489	5/2	2062.2865(3)	Flag; −0.14; 2062.228
2110.886.....	25000	47373.47	0	3/2	47373	1/2	2110.8858(3)	...
2134.273.....	700	46854.36	11419	3/2	58273[e]	3/2[f]	...	...
2165.064.....	70	46188.01	11419	3/2	57607[e]	1/2	...	...
2177.882.....	450	45916.17	0	3/2	45915	1/2	...	...
2177.895[h].....	950	45915.90	0	3/2	45915	1/2	2177.8956(3)	...
2177.907.....	500	45915.64	0	3/2	45915	1/2	...	...
2214.820.....	100	45150.40	11419	3/2	56569	3/2	2214.8188(25)	...
2228.902.....	900000	44865.14	0	3/2	44865	3/2	2228.9052(4)	...
2231.302.....	350000	44816.88	0	3/2	44816	5/2	2231.3041(4)	...
2277.261.....	400000	43912.40	0	3/2	43912	3/2	2277.2624(4)	...
2317.946.....	15	43141.64	11419	3/2	54560	1/2	2317.9484(4)	...
2349.734.....	15	42558.01	11419	3/2	53977	5/2	2349.7338(4)	...
2355.170.....	100	42459.78	11419	3/2	53878	3/2	2355.1694(4)	...
2401.61	400	41638.7	15437	5/2	57075	5/2	2401.6720(29)	Flag; 0.17; 2401.704
2431.19	70	41132.1	15437	5/2	56569	3/2	2431.1995(30)	Flag; 0.15; 2431.268
2448.778.....	150	40836.69	11419	3/2	52255	1/2	2448.7790(4)	Flag; −0.04
2497.67	5	40037.3	15437	5/2	55474	5/2	2497.6763(4)	Flag; 0.13; 2497.736
2516.390.....	1500	39739.47	11419	3/2	51158	5/2	2516.3908(4)	Complex; narrow
2525.250.....	4000	39600.04	11419	3/2	51019	3/2	2525.2493(5)	Complex; narrow
2594.73	40	38539.7	15437	5/2	53977	5/2	2594.7371(5)	Flag; 0.14; 2594.800
2601.36	20	38441.4	15437	5/2	53878	3/2	2601.3669(5)	Flag; 0.14; 2601.430
2628.688.....	150000	38041.79	11419	3/2	49460	3/2	2628.6825(5)	Complex; 0.14
2697.55	40000	37070.7	11419	3/2	48489	5/2	2697.5387(5)	Flag; −0.27; 2697.418
2731.223.....	20	36613.63	21660	1/2	58273[e]	3/2[f]	...	...
2731.300[h].....	40	36612.60	21660	1/2	58273[e]	3/2[f]	...	...
2731.376.....	20	36611.58	21660	1/2	58273[e]	3/2[f]	...	...
2781.297.....	35000	35954.45	11419	3/2	47373	1/2	2781.2978(5)	Complex; narrow
2781.929.....	5	35946.28	21660	1/2	57607[e]	1/2	...	...
2782.010[h].....	10	35945.24	21660	1/2	57607[e]	1/2	...	...
2782.090.....	5	35944.20	21660	1/2	57607[e]	1/2	...	...
2799.47	100	35721.0	15437	5/2	51158	5/2	2799.4742(5)	Flag; 0.16; 2799.547
2810.443.....	10000	35581.58	15437	5/2	51019	3/2	2810.4422(6)	Flag; 0.15; 2810.511
2864.532.....	250	34909.72	21660	1/2	56569	3/2	...	...
2864.628[h].....	550	34908.55	21660	1/2	56569	3/2	2864.6280(41)	...
2864.708.....	300	34907.57	21660	1/2	56569	3/2	...	...
2884.327.....	3	34670.13	21660	1/2	56329	3/2	...	...
2884.427[h].....	8	34668.93	21660	1/2	56329	3/2	2884.4162(6)	...
2884.487.....	5	34668.21	21660	1/2	56329	3/2	...	...
2898.814.....	150000	34496.87	11419	3/2	45915	1/2	2898.8159(6)	...

TABLE 1—*Continued*

λ_{vac}[a] (Å)	Int.	σ (cm^{-1})	Odd Level[b] (cm^{-1})	J_{odd}	Even Level[b] (cm^{-1})	J_{even}	λ_{calc}[c] (Å)	Comment[d]
2939.136.....	100000	34023.60	15437	5/2	49460	3/2	...	...
2939.156[h].....	200000	34023.37	15437	5/2	49460	3/2	2939.1529(6)	...
2939.176.....	100000	34023.14	15437	5/2	49460	3/2	...	...
2989.88	150000	33446.2	11419	3/2	44865	3/2	2989.8909(6)	Flag; −0.05
2994.20	6000	33397.9	11419	3/2	44816	5/2	2994.2090(6)	Flag; −0.05
3025.50	150000	33052.4	15437	5/2	48489	5/2	3025.5018(6)	Complex
3068.557.....	900000	32588.61	0	3/2	32588	1/2	...	...
3068.591[h].....	1500000	32588.25	0	3/2	32588	1/2	3068.5934(7)	...
3068.643.....	600000	32587.69	0	3/2	32588	1/2	...	...
3077.55	15000	32493.4	11419	3/2	43912	3/2	3077.5542(7)	Flag; −0.06; 3077.527
3112.996.....	70	32123.39	64711[i]	?	32588	1/2	...	...
3113.042[h].....	140	32122.92	64711[i]	?	32588	1/2	...	...
3113.087.....	70	32122.46	64711[i]	?	32588	1/2	...	...

Table 1 is also available in machine-readable form in the electronic edition of the *Astrophysical Journal*.

[a] Wavelength uncertainty is ±0.002 Å (one standard deviation) except in the case of complex lines for which only two decimal places are given. For these lines the uncertainty is ±0.01 Å.

[b] Levels and *J*-values taken from George et al. 1985 except as noted.

[c] Vacuum wavelength calculated from the level values of George et al. 1985.

[d] Comments give appearance of hyperfine structure, width of pattern in Å, and wavelength of leading components in Å, if it is resolved. Positive (negative) widths indicate that pattern is degraded to shorter (longer) wavelengths.

[e] Level taken from AEL (Moore 1958).

[f] *J*-value revised from AEL (Moore 1958) based on transition at 2731 Å.

[g] Level from Clearman 1952.

[h] Center of gravity of the resolved components based on their estimated intensities.

[i] Level from Mrozowski 1942.

Dworetsky (1982) identified seven lines of Bi II and determined an abundance enhancement of nearly 6 orders of magnitude relative to the solar system value. For only one other star, the magnetic chemically peculiar star HR 465 (Cowley 1987), had the detection of bismuth lines been reasonably well grounded prior to the launch of *HST*.

Guaranteed Time Observer (GTO) GHRS observations were designed to provide spectral data that would address the issues of the bismuth abundance for the ionization stages Bi^{+} and Bi^{++} and line blending in the vicinity of the strongest bismuth lines at ultraviolet wavelengths. The knowledge gained from these observations would then lay the groundwork for future study of bismuth in chemically normal and peculiar stars at ultraviolet wavelengths at lower spectral resolution (i.e., high-dispersion *IUE* data). However, in order to identify and model properly the bismuth features at the spectral resolution of the GHRS echelle mode, it was deemed necessary to obtain more accurate and extensive atomic data than were previously available. In this paper we present new laboratory wavelengths and hyperfine structures for strong lines of the first three ionization stages of bismuth at satellite ultraviolet wavelengths (1200–3300 Å) along with oscillator strengths calculated under the assumption of core-valence (CV) interaction. We apply these data to the determination of the bismuth abundance for the HgMn stars χ Lupi and HR 7775.

2. WAVELENGTH MEASUREMENTS AND HYPERFINE STRUCTURE

Spectra of Bi I, Bi II, and Bi III were obtained with the 10.7 m normal-incidence vacuum spectrograph at the National Institute of Standards and Technology. The grating was ruled with 1200 lines mm^{-1} and was blazed at 1200 Å in the first order. The plate factor in the first order was 0.78 Å mm^{-1}. A copper hollow cathode light source containing remnants of sputtered platinum from an earlier experiment and chips of metallic bismuth was operated at a direct current of 400 mA. The carrier gas consisted of a flowing mixture of four parts helium and one part neon at a total pressure of 320 Pa (2.4 torr). Photographic exposures ranging in time from 15 s to 60 minutes were made on 101-05 type plates in the region 380–3370 Å. Observations were made in the first order with filters to eliminate lines from higher grating orders. Lines of Cu II (Ross 1970) and Pt I, Pt II (Sansonetti et al. 1992) were used as the wavelength standards.

Tables 1–3 present our measured wavelengths and wavenumbers for the lines of Bi I, Bi II, and Bi III, respectively, along with the energy and angular momentum of the combining levels for each classified transition. From the standard deviation of the fits to the standard lines we estimate the uncertainty of the wavelengths (one standard uncertainty level) to be ±0.002 Å. The centers of gravity for some complex lines have larger uncertainties and are given with only two decimal places in the tables. The intensities are visual estimates of plate blackening.

The results for Bi I are complicated by the fact that many of the lines appear as partially resolved hyperfine structure (hfs) patterns. In Tables 1–3 we describe the lines as they appear at our laboratory resolving power ($R = \lambda/\Delta\lambda = 150,000$). Since the resolving power of the GHRS is somewhat lower ($R = 90{,}000$), the hyperfine structure will appear slightly less well resolved in the stellar spectrum. For lines that appear as flag patterns we give the wavelength of the center of gravity in the main part of the table. In the comments column we note the appearance of the line as a flag and give the total width of the pattern in Å as well as the wavelength of the leading hyperfine component. Lines with negative widths are degraded to the red. Further details of

TABLE 2

WAVELENGTHS FOR Bi II

λ_{vac}[a] (Å)	Int.	σ (cm^{-1})	Even Level (cm^{-1})	J_{even}	Odd Level (cm^{-1})	J_{odd}	Comments[b]
1058.846	300	94442.44	0	0	94440	1	...
1085.465	100	92126.42	17030	2	109157	2	...
1097.755	25	91095.01	17030	2	108126	1	...
1099.174	300	90977.41	17030	2	108007	3	...
1112.523	120	89885.78	0	0	89883	1	...
1116.327	20	89579.49	17030	2	106611	1	...
1123.517	250	89006.22	13324	1	102330	2	...
1129.998	18	88495.73	17030	2	105526	2	...
1147.190	250	87169.52	13324	1	100492	1	...
1163.171	700	85971.88	17030	2	103003	3	...
1167.056	800	85685.69	13324	1	99011	2	...
1172.334	120	85299.92	17030	2	102330	2	...
1186.118	30	84308.64	17030	2	101341	1	...
1198.133	300	83463.19	17030	2	100492	1	...
1219.813	40	81979.78	17030	2	99011	2	...
1225.412	800	81605.21	13324	1	94928	2	...
1232.792	100	81116.68	13324	1	94440	1	Complex
1241.045	5000	80577.26	0	0	80575	1	...
1265.331	250	79030.70	17030	2	96057	3	...
1283.715	3000	77898.91	17030	2	94298	2	...
1306.161	400	76560.24	13324	1	89883	1	...
1316.943	80	75933.43	...	...	...	...	New line
1317.066	60	75926.34	...	...	...	...	...
1317.167	50	75920.52	...	...	...	...	...
1325.450	900	75446.07	13324	1	88769	2	Complex
1329.444	600	75219.42	33936	2	109157	2	Complex
1347.925	40	74188.10	33936	2	108126	1	...
1350.068	800	74070.34	33936	2	108007	3	...
1372.609	800	72853.96	17030	2	89883	1	...
1376.036	80	72672.52	33936	2	106611	1	...
1393.926	1800	71739.82	17030	2	88769	2	...
1396.872	50	71588.52	33936	2	105526	2	...
1436.7768[c]	2000	69600.233	0	0	69598	1	...
1436.8205[c]	1700	69598.116	0	0	69598	1	...
1436.8564[c]	1300	69596.377	0	0	69598	1	...
1447.914	100	69064.88	33936	2	103003	3	...
1455.091	3500	68724.22	13324	1	82047	2	...
1462.138	500	68393.00	33936	2	102330	2	...
1486.943	250	67252.07	13324	1	80575	1	...
1486.963	300	67251.17	13324	1	80575	1	...
1502.488	90	66556.27	33936	2	100492	1	...
1520.549	600	65765.72	13324	1	79089	2	Flag; −0.06; 1520.520
1533.139	4000	65225.66	17030	2	82255	3	...
1536.745	40	65072.60	33936	2	99011	2	...
1538.037	250	65017.94	17030	2	82047	2	...
1563.649	100	63952.97	44173	0	108126	1	...
1573.632	20	63547.26	17030	2	80575	1	...
1573.673	30	63545.60	17030	2	80575	1	...
1573.721	50	63543.66	17030	2	80575	1	...
1591.668	1000	62827.17	13324	1	76147	2	...
1591.741	800	62824.29	13324	1	76147	2	...
1591.803	600	62821.84	13324	1	76147	2	...
1591.853	500	62819.87	13324	1	76147	2	...
1591.891	300	62818.37	13324	1	76147	2	...
1601.602	100	62437.48	44173	0	106611	1	...
1609.629	115	62126.12	33936	2	96057	3	Flag; −0.14
1609.665	100	62124.73	33936	2	96057	3	...
1609.696	85	62123.53	33936	2	96057	3	...
1609.723	70	62122.49	33936	2	96057	3	...
1609.748	60	62121.52	33936	2	96057	3	...
1609.762	70	62120.98	33936	2	96057	3	Unresolved tail
1611.358	2000	62059.46	17030	2	79089	2	...
1691.57	100	59116.7	17030	2	76147	2	Complex; 0.17
1749.232	25	57167.95	44173	0	101341	1	...
1749.279	15	57166.41	44173	0	101341	1	...

TABLE 2—*Continued*

λ_{vac}[a] (Å)	Int.	σ (cm^{-1})	Even Level (cm^{-1})	J_{even}	Odd Level (cm^{-1})	J_{odd}	Comments[b]
1749.316.....	10	57165.20	44173	0	101341	1	...
1775.54	3	56320.9	44173	0	100492	1	Complex
1776.991.....	1500	56274.91	13324	1	69598	1	...
1777.057.....	600	56272.82	13324	1	69598	1	...
1777.078.....	600	56272.15	13324	1	69598	1	...
1777.122.....	1000	56270.76	13324	1	69598	1	...
1787.406.....	4000	55947.00	33936	2	89883	1	...
1791.842.....	15000	55808.49	13324	1	69133	0	...
1823.728.....	2000	54832.74	33936	2	88769	2	Complex
1902.341[d].....	15000	52566.81	17030	2	69598	1	Complex; 0.14
1989.250.....	3	50270.20	44173	0	94440	1	...
1989.305.....	4	50268.81	44173	0	94440	1	...
1989.374.....	5	50267.07	44173	0	94440	1	...
2069.598.....	10	48318.56	33936	2	82255	3	Complex; 0.09
2144.105.....	6	46639.51	33936	2	80575	1	...
2144.150.....	8	46638.53	33936	2	80575	1	...
2144.203.....	10	46637.38	33936	2	80575	1	...
2187.610.....	120	45711.99	44173	0	89883	1	...
2214.680.....	12	45153.25	33936	2	79089	2	...
2214.713.....	10	45152.58	33936	2	79089	2	...
2214.738.....	9	45152.07	33936	2	79089	2	...
2214.760.....	8	45151.62	33936	2	79089	2	...
2368.916.....	120	42213.40	33936	2	76147	2	...
2369.053.....	110	42210.96	33936	2	76147	2	...
2369.170.....	100	42208.87	33936	2	76147	2	...
2369.266.....	90	42207.16	33936	2	76147	2	...
2369.339.....	80	42205.86	33936	2	76147	2	...
2480.815.....	8	40309.33	109904	2	69598	1	...
2480.905.....	10	40307.87	109904	2	69598	1	...
2481.018.....	12	40306.04	109904	2	69598	1	...
2501.758.....	4	39971.89	13324	1	69133	0	...
2501.771.....	5	39971.68	13324	1	69133	0	...
2501.794.....	6	39971.32	13324	1	69133	0	...
2503.280.....	10	39947.59	116089	3	76147	2	...
2503.384.....	12	39945.93	116089	3	76147	2	...
2503.527.....	12	39943.65	116089	3	76147	2	Double
2503.692.....	15	39941.02	116089	3	76147	2	Shaded to blue
2503.887.....	20	39937.90	116089	3	76147	2	...
2714.036.....	300	36845.50	115933	3	79089	2	...
2804.161.....	40	35661.29	33936	2	69598	1	...
2804.312.....	35	35659.37	33936	2	69598	1	...
2804.433.....	30	35657.83	33936	2	69598	1	...
2806.049.....	80	35637.30	116212	2	80575	1	Complex; 0.06
2817.733.....	10	35489.52	105083	2	69598	1	Perturbed by Pt
2817.900.....	12	35487.42	105083	2	69598	1	...
2818.082.....	15	35485.13	105083	2	69598	1	...
2937.60	40	34041.4	116089	3	82047	2	Flag; 0.30; 2937.742
2951.277.....	150	33883.64	115933	3	82047	2	...
3111.756.....	4	32136.20	108278	3	76147	2	...
3111.888.....	5	32134.83	108278	3	76147	2	...
3112.056.....	8	32133.10	108278	3	76147	2	...
3112.262.....	11	32130.97	108278	3	76147	2	...
3112.507.....	15	32128.44	108278	3	76147	2	...
3117.736.....	10	32074.56	112645	0	80575	1	...
3117.829.....	8	32073.60	112645	0	80575	1	...
3117.905.....	7	32072.82	112645	0	80575	1	...

Table 2 is also available in machine-readable form in the electronic edition of the *Astrophysical Journal*.

[a] Wavelength uncertainty is ± 0.002 Å except in the case of complex lines for which only two decimal places are given. For these lines the uncertainty is ± 0.01 Å.

[b] Comments give appearance of hyperfine structure, width of pattern in Å, and wavelength of leading component in Å, if it is resolved. Positive (negative) widths indicate that the pattern is degraded to shorter (longer) wavelengths.

[c] Wavelength uncertainty ± 0.0010 Å.

[d] Center of gravity calculated from data of Wahlgren et al. 1994b.

TABLE 3

WAVELENGTHS FOR Bi III

λ_{vac}[a] (Å)	Int.	σ (cm^{-1})	Odd Level (cm^{-1})	J_{odd}	Even Level (cm^{-1})	J_{even}	Comments
1051.787	3	95076.28	0	1/2	95075	1/2	...
1145.903	3	87267.42	20788	3/2	108052	1/2	...
1145.937	2	87264.83	20788	3/2	108052	1/2	...
1204.234	2	83040.34	0	1/2	83038	3/2	...
1204.277	1.6	83037.37	0	1/2	83038	3/2	...
1204.310	1.2	83035.10	0	1/2	83038	3/2	...
1224.617	150	81658.18	20788	3/2	102446	5/2	...
1326.848	200	75366.58	20788	3/2	96154	3/2	...
1346.088	60	74289.35	20788	3/2	95075	1/2	...
1346.124	50	74287.36	20788	3/2	95075	1/2	...
1423.3081[b].....	120	70258.857	0	1/2	70254	1/2	...
1423.3565[b].....	90	70256.468	0	1/2	70254	1/2	...
1423.4806[b].....	70	70250.343	0	1/2	70254	1/2	...
1423.5290[b].....	120	70247.954	0	1/2	70254	1/2	...
1460.846	80	68453.49	20788	3/2	89236	5/2	...
1460.920	70	68450.02	20788	3/2	89236	5/2	...
1460.985	60	68446.97	20788	3/2	89236	5/2	...
1461.038	50	68444.49	20788	3/2	89236	5/2	...
1461.079	40	68442.57	20788	3/2	89236	5/2	Perturbed by Pt
1461.112	30	68441.02	20788	3/2	89236	5/2	...
1606.343	80	62253.20	20788	3/2	83038	3/2	...
1606.419	70	62250.26	20788	3/2	83038	3/2	...
1606.484	60	62247.74	20788	3/2	83038	3/2	...
1606.535	50	62245.76	20788	3/2	83038	3/2	...
2021.457	6	49469.27	20788	3/2	70254	1/2	...
2021.797[c]	5	49460.95	20788	3/2	70254	1/2	Blend with Bi I
2073.555	8	48226.36	137455	7/2	89236	5/2	...
2073.619	5	48224.87	137455	7/2	89236	5/2	...
2073.710	12	48222.75	137455	7/2	89236	5/2	Perturbed
2073.828	10	48220.01	137455	7/2	89236	5/2	...
2073.950	12	48217.17	137455	7/2	89236	5/2	...
2074.105	...	48213.57	137455	7/2	89236	5/2	Perturbed by Cu
2415.380	25	41401.35	137555	5/2	96154	3/2	...
2415.411	20	41400.82	137555	5/2	96154	3/2	...
2415.436	15	41400.39	137555	5/2	96154	3/2	Perturbed
2415.448	10	41400.19	137555	5/2	96154	3/2	Unresolved
2856.238	4	35011.09	137455	7/2	102446	5/2	...
2856.273	5	35010.66	137455	7/2	102446	5/2	...
2856.319	7	35010.10	137455	7/2	102446	5/2	...
2856.377	9	35009.38	137455	7/2	102446	5/2	...
2856.448	12	35008.51	137455	7/2	102446	5/2	...
2856.530	15	35007.51	137455	7/2	102446	5/2	...

Table 3 is also available in machine-readable form in the electronic edition of the *Astrophysical Journal.*

[a] Wavelength uncertainty is ± 0.002 Å.

[b] Wavelength uncertainty is ± 0.0010 Å.

[c] Line not observed owing to blend. Wavelength based on calculated interval from $\lambda 2021.457$ of 8.32 cm^{-1} derived from the values in Tables 3 and 6. Intensity based on theoretical ratios of the hyperfine components.

the hfs of many of the lines are given by Mrozowski (1942). For some lines we have made use of Mrozowski's measurements for the widths of the patterns.

Precise measurements of the spectrum of Bi I in the infrared using a Fourier transform spectrometer have been reported by George, Munsee, & Vergès (1985). Based on these observations they gave revised values for some levels of neutral bismuth with an uncertainty estimated to be less than 0.005 cm^{-1}. From their level values we have calculated wavelengths for many of the ultraviolet lines observed in this work. The calculated wavelengths are reported for comparison with our measurements in Table 1. Approximately 20 of the lines reported in Table 1 were observed in absorption by Mathews et al. (1989). These authors estimate the uncertainty of their measurements to be ± 0.09 cm^{-1} and comment that there is a possible bias in the data toward the negative end of the uncertainty range. This bias is confirmed by our wavelengths, which are systematically shorter than those of Mathews et al. (1989) by approximately 0.003 Å.

For Bi II and Bi III the hfs splittings are greater than for Bi I, and we thus give the wavelengths of all of the observed components. Most of the lines were originally reported by Crawford & McLay (1934), although a few are newly presented here. Figures 1 and 2 display tracings of the newly acquired photographic plate data for Bi II $\lambda 1436.8$ and Bi III $\lambda 1423.4$, respectively, two of the main lines of astrophysical interest in the present study. In both figures the hyperfine components are clearly resolved. Measurement of each of these components can be made to an estimated uncertainty of 1 mÅ.

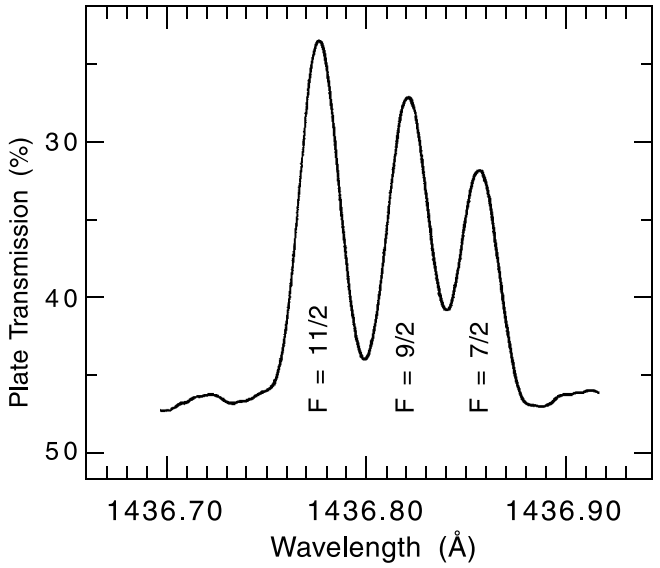

FIG. 1.—Microdensitometer trace of the Bi II $6p^2\ ^3P_0$ [$F' = 9/2$]–$6p7s\ ^3P_1$ [F] transition (λ1436) as observed photographically in the laboratory.

3. ATOMIC CALCULATIONS

Complex systems with nuclear charge as high as bismuth require a careful treatment of both electron correlation and relativistic effects. Recently, we have investigated different computational approaches (Brage, Leckrone, & Froese Fischer 1996; Brage, Proffitt, & Leckrone 1998a, 1999), mainly based on the multiconfiguration Dirac-Fock (MCDF) method (Grant et al. 1980) in the form of the GRASP_VU code (Parpia, Froese Fischer, & Grant 1996). From this and similar work it is clear that systematic and large-scale calculations are necessary to obtain reliable results. For the ions Bi^+ and Bi^{++} we have computed both oscillator strengths and hfs constants. For the latter we have applied software developed by Jönsson, Parpia, & Froese Fischer (1996).

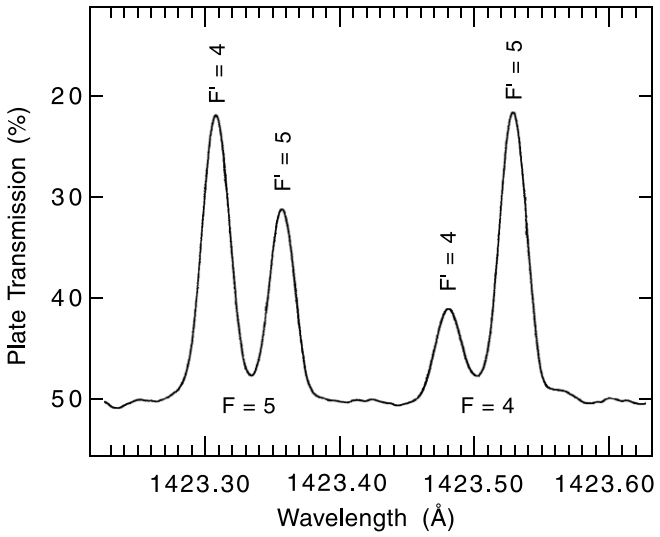

FIG. 2.—Microdensitometer trace of the Bi III $6s^26p\ ^2P_{1/2}$ [F']–$6s6p^2\ ^4P_{1/2}$ [F] transition (λ1423) as observed photographically in the laboratory.

3.1. *The MCDF Method*

The codes in the GRASP family are based on the MCDF method (Grant et al. 1980; McKenzie, Grant, & Norrington 1980). Our approach is commonly referred to as Dirac-Coulomb, since the Hamiltonian defining the variational method is written as

$$H_{\rm DC} = \sum_i \left(\alpha_i \cdot \boldsymbol{p}_i c + \beta_i c^2 - \frac{Z}{r_i} \right) + \sum_{i \neq j} \frac{1}{r_{ij}} , \qquad (1)$$

with standard notations. The first part is a sum over single-particle Dirac Hamiltonians, while the second represents the instantaneous Coulomb potential. The trial functions are expansions over configuration state functions (CSFs), $\Phi_j(\alpha_j J)$,

$$\Psi(\gamma J) = \sum_j c_j \Phi_j(\alpha_j J) , \qquad (2)$$

where α_j represents all other quantum numbers needed to define uniquely the CSFs (Grant 1988). The label γ for the atomic state function (ASF), $\Psi(\gamma J)$, is usually chosen as the α_j of the CSF with largest weight, $|c_j|$ in the expansion above. However, in this paper we will use the same labels as in the experimental investigation, based on the *LS* coupling, instead of the *jj* coupling used to construct the relativistic CSFs.

To set up the system of integrodifferential equations according to the MCDF method, we need to define an energy functional to optimize. In this paper we use the extended optimal level (EOL) scheme, where the functional is

$$F = \frac{\sum_k (2J_k + 1) E_k(\gamma_k J_k)}{\sum_k (2J_k + 1)} , \qquad (3)$$

i.e., the weighted (with $2J_k + 1$, where J_k is the total angular momentum) sum of the energies $[E_k(\gamma_k J_k)]$ of a set of ASFs, defined by the labels $\{\gamma_k J_k\}$.

The influence of corrections to the Dirac-Coulomb Hamiltonian, in the form of the Breit interaction, was considered in calculations for similar systems (Brage et al. 1996). It was found that they contribute less than 1% to the oscillator strengths for heavy ions of low-ionization states.

3.2. *Computational Strategies*

In our earlier work it was shown that in relatively simple systems and for states with low-excitation energies, the systematic restricted active space (RAS) calculations can be used and pushed to a convergence, accounting for a number of different types of correlation. In more complex systems, and for higher excitation energies, this method was modified invoking first-order calculations, where the full interaction matrix was only set up for a subset of the CSFs. As a first step only first-order interaction was included for the large CSF set. By using condensation techniques, where all CSFs with a weight smaller than a certain cutoff are omitted, the size of the calculations can be drastically limited, while still including all important contributions.

In this work we encounter two different ionic systems, Bi^+ and Bi^{++}. The latter is a three-electron system outside closed core subshells, and we are in this case mainly interested in the lowest odd and even levels. This makes it possible to use the RAS technique with only slight modifications when including CV correlation. The ion Bi^+ is a

more complex four-valence electron system, and for this system we use a more approximate approach to the handling of the larger number of configurations and hence to a slower convergence as a function of the number of included orbitals.

3.3. *Calculations for* Bi III

For Bi III we are interested in resonance transitions between the terms $6s^26p\ ^2P$ and $6s6p^2\ ^4P$. The EOL functional is therefore defined according to the reference states $6s^26p\ ^2P_{1/2,\,3/2}$, $6s6p^2\ ^4P_{1/2,\,3/2,\,5/2}$. From a predefined set of orbitals, usually labeled an active set, we can now generate all possible CSFs under certain constraints, with the same parity and J-values as the CSFs in the reference set. By increasing the size of the active set in a systematic way, we may investigate the convergence of our approach. In Table 4 we list the results with different sizes of active sets of orbitals.

The first goal is to investigate the valence correlation, i.e., the correlation between the outer three electrons. We are here able to apply a systematic approach, where the active set is increased in four steps, as shown in Table 4. We can see that the excitation energies do converge, albeit to values that are too low. In a final attempt to model the energy spectrum, we add (CV) correlation, by including CSFs with one hole in the 5*d* core subshell and four outer electrons. This improves the excitation energies, and the fine structure of the ground term is now in excellent agreement with experiment.

The resulting *gf*-values are given in Table 5. Some instabilities are clear for the first calculations. These can be understood from the fact that the transitions we investigate are basically intercombination lines. In a quasi-relativistic treatment (solving the Schrödinger equation and including Breit-Pauli interaction as perturbations) they would be induced by spin-dependent interaction between the $6s6p^2\ ^4P$ term and different doublets of the same configuration. The computed oscillator strengths are therefore very sensitive to the relative positions of the terms within the $6s6p^2$ configuration. It requires quite a large active set of orbitals to represent this term splitting correctly. In the relativistic approach, this complication is represented by a cancellation of different large contributions to the line strengths of the intercombination transitions. In spite of these complications, it is clear that the valence correlation result, at least for the stronger lines, is approaching convergence.

The *gf*-values can be computed using two different forms for the transition operator, the Babushkin and the Coulomb form. In the nonrelativistic limit these converge to the length and velocity forms, respectively. It is well known that for relatively weak transitions, the convergence of the Coulomb form is very slow. We therefore use the Babushkin form all through our calculations. The *gf*-values do depend on the line strength and the transition energy. As is common in this kind of calculation, we use theoretical line strengths but experimental transition energies.

We give the results for the magnetic dipole and electric quadrupole hfs constants (labeled A and B) in Table 6 and

TABLE 4

ENERGY LEVELS IN Bi III

	Excitation Energies (cm^{-1})				
	$6s^26p\ ^2P$		$6s6p^2\ ^4P$		
Active Set	$J = 1/2$	$J = 3/2$	$J = 1/2$	$J = 3/2$	$J = 5/2$
Dirac-Fock[a]	0	20287	62012	73484	82797
6*s*, 6*p*, 6*d*, 6*f*, 6*g*	0	20228	64072	80394	83223
7*s*, 7*p*, 7*d*	0	20094	65008	76822	83887
8*s*, 8*p*, 8*d*	0	20091	65086	76911	83944
9*s*, 9*p*, 9*d*	0	20090	65100	76921	83953
Including CV[b]	0	20744	67525	80008	87369
Experiment[c]	0	20788	70254	83038	89236

[a] Single-configuration Dirac-Fock calculation.
[b] Core-valence correlation (see text).
[c] See Table 3.

TABLE 5

COMPUTED[a] *gf*-VALUES FOR SELECT Bi III TRANSITIONS

Active Set	$^2P^o_{1/2}-{}^4P_{1/2}$ 1423 Å	$^2P^o_{1/2}-{}^4P_{3/2}$ 1204 Å	$^2P^o_{3/2}-{}^4P_{1/2}$ 2022 Å	$^2P^o_{3/2}-{}^4P_{3/2}$ 1606 Å	$^2P^o_{3/2}-{}^4P_{5/2}$ 1461 Å
Dirac-Fock	6.72E−2	1.98E−2	5.19E−3	1.46E−2	2.06E−1
6*s*, 6*p*, 6*d*, 6*f*, 6*g*	6.15E−2	3.72E−2	1.01E−2	1.36E−1	9.33E−2
7*s*, 7*p*, 7*d*	6.56E−2	2.73E−3	8.71E−3	1.24E−2	3.19E−2
8*s*, 8*p*, 8*d*	6.72E−2	2.16E−3	9.25E−3	1.15E−2	2.84E−2
9*s*, 9*p*, 9*d*	6.75E−2	1.65E−3	9.36E−3	1.07E−2	2.73E−2
CV[b]	6.45E−2	2.26E−3	6.57E−3	1.51E−2	6.92E−2

[a] Using ab initio line strengths and experimental wavelengths.
[b] Including core-valence correlation.

TABLE 6

HYPERFINE STRUCTURE CONSTANTS[a] FOR Bi III

	$6s^26p\ ^2P$			$6s6p^2\ ^4P$				
	$J = 1/2$	$J = 3/2$		$J = 1/2$	$J = 3/2$		$J = 5/2$	
ACTIVE SET	A	A	B	A	A	B	A	B
Dirac-Fock	13993	1186	−1233	41614	14378	−1047	14858	1346
6*s*, 6*p*, 6*d*, 6*f*, 6*g*	13585	1334	−1213	42690	14034	−1000	14605	771
7*s*, 7*p*, 7*d*	13057	536	−1093	43553	14042	−1022	14355	734
8*s*, 8*p*, 8*d*	13313	533	−1111	43377	13908	−1022	14262	702
9*s*, 9*p*, 9*d*	13204	531	−1103	43450	13899	−1021	14261	706
CV[b]	13502	647	−1146	46592	14401	−1024	14884	662
Experiment	14320[c]	...	...	51050[c]	15000[d]	...	15000[d]	...

[a] Hyperfine electric dipole (A) and magnetic quadrupole (B) constants presented in units of MHz.
[b] Including core-valence correlation.
[c] Measured value from λ1423, uncertainty 80 MHz.
[d] Crawford & McLay 1934.

the hyperfine induced wavelength splittings in Table 7. From Table 6 it is clear that the valence correlation calculations have converged to within a few percent. The inclusion of core-valence correlation increases the values of A and B, in most cases, by a fairly small amount. Looking at the splitting in wavelengths, shown in Table 7, experiment and theory agree to within a few percent. This agreement provides additional support for the accuracy of our calculations.

3.4. *Calculations for* Bi II

The four-electron system of Bi II is an even greater challenge to atomic calculations. Henderson et al. (1996) measured the lifetimes of some of the upper levels, which makes it possible to make some comparisons. There are no measured branching ratios, however, and as we will see below, the measured lifetimes do lead to some contradictions when compared to our calculations. A number of calculations have been performed for this system (e.g., Biéron, Marcinek, & Migdalek 1991), and we refer the reader to Henderson et al. (1996) for a more complete discussion.

The ground configuration of Bi^+ is $6s^26p^2$, while the first excited odd levels belong to the $6s6p^3$, $6s^26p7s$, and $6s^26p6d$ configurations. We use a technique in which we stepwise include one, two, and three configurations, and finally all configurations as obtained from a multireference set, single

TABLE 7

HYPERFINE STRUCTURE SPLITTING FOR Bi III

Transition	F_{lower}	F_{upper}	Theoretical λ[a] (Å)	Experimental λ (Å)
$6s^26p\ ^2P^o_{1/2}$–$6s6p^2\ ^4P_{1/2}$	4	5	1423.3081	1423.3081
	5	5	1423.3537	1423.3565
	4	4	1423.4655	1423.4806
	5	4	1423.5111	1423.5290
$6s^26p\ ^2P^o_{3/2}$–$6s6p^2\ ^4P_{3/2}$	5	6	1606.343	1606.343
	6	6	1606.346	
	4	5	1606.414	
	5	5	1606.417	1606.419
	6	5	1606.420	
	3	4	1606.474	
	4	4	1606.476	1606.484
	5	4	1606.480	
	3	3	1606.524	1606.535
	4	3	1606.526	
$6s^26p\ ^2P^o_{3/2}$–$6s6p^2\ ^4P_{5/2}$	6	7	1460.846	1460.846
	5	6	1460.918	1460.920
	6	6	1460.920	
	4	5	1460.979	
	5	5	1460.981	1460.985
	6	5	1460.984	
	3	4	1461.029	
	4	4	1461.032	1461.038
	5	4	1461.034	
	3	3	1461.071	1461.079
	4	3	1461.074	
	3	2	1461.103	1461.112

[a] Shortest wavelength in each transition array affixed to experimental value.

TABLE 8

EOL Functional States for Bi II

Parity	J	Level Designation
Even.....	0	$6s^26p^2\ ^3P_0$, $6s^26p^2\ ^1S_0$
Even.....	1	$6s^26p^2\ ^3P_1$
Even.....	2	$6s^26p^2\ ^3P_2$, $6s^26p^2\ ^1D_2$
Odd	0	$6s^26p7s\ ^3P_0$
Odd	1	$6s^26p7s\ ^3P_1$, $6s^26p6d\ ^3D_1$, $6s^26p7s\ ^1P_1$
Odd	2	$6s6p^3\ ^5S_2$, $6s^26p6d\ ^3D_2$, $6s^26p6d\ ^3F_2$, $6s^26p7s\ ^3P_2$

and double replacement calculation. The multireference set includes all levels with a given J-value belonging to the $\{6s^26p^2, 6s6p^26d, 6p^4\}$ set for the even configurations and the $\{6s6p^3, 6s^26p6d, 6s^26p7s\}$ set for the odd. The orbitals are optimized by using the EOL technique, on an energy functional composed of the equally weighted total energies of a reference set of states (Table 8). A separate calculation was performed for each pair of J-values. From the reference set, we generated new CSFs by single and double replacements of orbitals to a virtual orbital set, $\{6s, 6p, 6d, 5f, 7s\}$. Table 9 gives the resulting oscillator strengths, Table 10 compares our transition rates with previous determinations, and Table 11 gives an example of a hyperfine transition array.

One of the most interesting results of our calculations is related to branching ratios (the ratio of the transition rates of two lines with a common upper level) of two transitions involving the upper level $6s^26p7s\ ^3P_1$. In an earlier treatment of Bi II lines (Henderson et al. 1996), labeled NICA in Table 10, the predicted branching ratio between the two resonance lines at 1902.31 Å ($6s^26p^2\ ^3P_2$–$6s^26p7s\ ^3P_1$) and 1436.83 Å ($6s^26p^2\ ^3P_2$–$6s^26p7s\ ^3P_1$) was almost unity (0.35/0.34). This is in sharp contrast to that predicted from the MCDF calculations presented here (first set of results in Table 4), which gives a value close to 2 (0.37/0.18). This difference is completely attributed to relativistic effects, and

TABLE 9

Computed gf-Values for Bi II

λ_{vac}[a] (Å)	Designation	E_{low}[b] (cm^{-1})	gf_{th}[c]	gf_{sc}[d]
1112.5.....	$6s^26p^2\ ^3P_0$–$6s^26p7s\ ^1P_1$	0	0.08	...
1241.0.....	$6s^26p^2\ ^3P_0$–$6s^26p6d\ ^3D_1$	0	0.12	...
1436.8.....	$6s^26p^2\ ^3P_0$–$6s^26p7s\ ^3P_1$	0	0.17	0.21
1306.2.....	$6s^26p^2\ ^3P_1$–$6s^26p7s\ ^1P_1$	13324	0.08	...
1325.4.....	$6s^26p^2\ ^3P_1$–$6s^26p7s\ ^3P_2$	13324	0.34	...
1486.9.....	$6s^26p^2\ ^3P_1$–$6s^26p6d\ ^3D_1$	13324	0.055	...
1455.1.....	$6s^26p^2\ ^3P_1$–$6s^26p6d\ ^3F_2$	13324	0.65	...
1520.5.....	$6s^26p^2\ ^3P_1$–$6s^26p6d\ ^3D_2$	13324	0.007	...
1591.8.....	$6s^26p^2\ ^3P_1$–$6s6p^3\ ^5S_2$	13324	0	...
1777.1.....	$6s^26p^2\ ^3P_1$–$6s^26p7s\ ^3P_1$	13324	0.16	0.19
1791.8.....	$6s^26p^2\ ^3P_1$–$6s^26p7s\ ^3P_0$	13324	0.30	0.31
1372.6.....	$6s^26p^2\ ^3P_2$–$6s^26p7s\ ^1P_1$	17030	0.10	...
1393.9.....	$6s^26p^2\ ^3P_2$–$6s^26p7s\ ^3P_2$	17030	0.13	...
1538.0.....	$6s^26p^2\ ^3P_2$–$6s^26p6d\ ^3F_2$	17030	0.04	...
1573.7.....	$6s^26p^2\ ^3P_2$–$6s^26p6d\ ^3D_1$	17030	0.045	...
1611.4.....	$6s^26p^2\ ^3P_2$–$6s^26p6d\ ^3D_2$	17030	0.17	...
1691.6.....	$6s^26p^2\ ^3P_2$–$6s6p^3\ ^5S_2$	17030	0.005	...
1902.3.....	$6s^26p^2\ ^3P_2$–$6s^26p7s\ ^3P_1$	17030	0.60	0.73
1787.4.....	$6s^26p^2\ ^1D_2$–$6s^26p7s\ ^1P_1$	33936	0.95	...
1823.7.....	$6s^26p^2\ ^1D_2$–$6s^26p7s\ ^3P_2$	33936	0.001	...
2078.5.....	$6s^26p^2\ ^1D_2$–$6s^26p6d\ ^3F_2$	33936	0.008	...
2144.1.....	$6s^26p^2\ ^1D_2$–$6s^26p6d\ ^3D_1$	33936	0	...
2214.7.....	$6s^26p^2\ ^1D_2$–$6s^26p6d\ ^3D_2$	33936	0.009	...
2369.0.....	$6s^26p^2\ ^1D_2$–$6s6p^3\ ^5S_2$	33936	0.004	...
2804.3.....	$6s^26p^2\ ^1D_2$–$6s^26p7s\ ^3P_1$	33936	0.01	0.01
2187.6.....	$6s^26p^2\ ^1S_0$–$6s^26p7s\ ^1P_1$	44173	0.15	...
3933.1.....	$6s^26p^2\ ^1S_0$–$6s^26p7s\ ^3P_1$	44173	0.001	0.001

[a] Approximate wavelength; exact wavelengths with hyperfine structure are given in Table 2.

[b] Excitation energy of lower state.

[c] "Theoretical" gf-value computed using the Babushkin form of line strength and experimental wavelengths.

[d] "Scaled" gf-value computed using a theoretical branching ratio and experimental lifetime (Hendersson et al. 1996).

TABLE 10

Rates for $6s^26p^2$–$6s^26p7s$ Transitions in Bi II

Transition	λ_{vac}[a] (Å)	Rates (ns^{-1}) Type I[b] MCDF[d]	Type I[b] RICA[e]	Type II[c] MCDF[d]	Type II[c] RICA[e]	Type II[c] NICA[f]
$6s^26p^2\ ^3P_1$–$6s^26p7s\ ^3P_0$	1791.8	0.62	0.62	0.64	0.64	0.64
$6s^26p^2\ ^3P_0$–$6s^26p7s\ ^3P_1$	1436.8	0.18	0.16	0.22	0.20	0.34
$6s^26p^2\ ^3P_1$–$6s^26p7s\ ^3P_1$	1777.1	0.11	0.10	0.13	0.13	0.10
$6s^26p^2\ ^3P_2$–$6s^26p7s\ ^3P_1$	1902.3	0.37	0.37	0.45	0.47	0.35
$6s^26p^2\ ^1D_2$–$6s^26p7s\ ^3P_1$	2804.3	0.003	0.003	0.004	0.004	0.003
$6s^26p^2\ ^1S_0$–$6s^26p7s\ ^3P_1$	3933.1	0.0001	0.0002	0.0001	0.0002	0.0004
BR($^3P_2/^3P_0$)[g]	...	2.1	2.3	2.1	2.3	1.0

[a] Approximate wavelength.

[b] Assuming computed lifetimes [$\tau(^3P_1) = 1.50$ ns and $\tau(^3P_0) = 1.61$ ns].

[c] Assuming measured lifetimes, from Henderson et al. 1996 [$\tau(^3P_1) = 1.24$ ns and $\tau(^3P_0) = 1.56$ ns].

[d] Branching ratios from MCDF calculations.

[e] Branching ratios from Relativistic Intermediate Coupling Amplitude calculations by Curtis et al. 1997.

[f] Branching ratios from Nonrelativistic Intermediate Coupling Amplitude calculations by Henderson et al. 1996.

[g] Branching ratio for $6s^26p^2\ ^3P_2$–$6s^26p7s\ ^3P_1$ (1902.3 Å) and $6s^26p^2\ ^3P_0$–$6s^26p7s\ ^3P_1$ (1436.8 Å)

TABLE 11

HYPERFINE STRUCTURE IN Bi II λ1902.3

F_l	F_u	λ_{vac} (Å)	*gf*-Value
4.5.....	5.5	1902.265	0.016
5.5.....	5.5	1902.288	0.071
6.5.....	5.5	1902.314	0.203
3.5.....	4.5	1902.325	0.045
4.5.....	4.5	1902.343	0.094
5.5.....	4.5	1902.365	0.103
2.5.....	3.5	1902.374	0.087
3.5.....	3.5	1902.388	0.071
4.5.....	3.5	1902.407	0.035

the disagreement between the two results initiated a separate study (Curtis et al. 1997), where relativistic effects were added to the method used by Henderson et al. (1996). These methods can only predict branching ratios and rely on experimental lifetimes to deduce the final transition rates. We now discuss the results from these different studies.

With reference to Table 10, if we start by looking at the branching ratios, it is clear that the relativistic effects drastically change the values for some of the levels and that our calculations do agree with the ones by Curtis et al. (1997). If we then look at the lifetimes, we find a good agreement between the experiment by Henderson et al. (1996; 1.61 ns) and the present calculations (1.56 ns) for the $6s^2 6p7s\ ^3P_0$ level. On the other hand, for $6s^2 6p7s\ ^3P_1$, experiment (1.24 ns) and our theory (1.50 ns) differ by about 20%. It is instructive to compare the first set of results in Table 10 (type I, MCDF), which corresponds to ab initio calculations, with the fourth (type II, RICA), which corresponds to experimental lifetime and computed branching ratio. By comparing the relative difference as a function of transition rate magnitude for the four strongest lines, it is clear that the disagreement for the λ1902 line stands out as comparatively large. This result is against our common experience that we should do better for stronger than for weaker lines.

In conclusion, we combine experimental lifetimes and theoretical branching ratios to deduce the *gf*-values for our synthetic spectra (see last column of Table 9 and type II MCDF results in Table 10), but we caution against a too high confidence level on the experimental lifetime for the $6s^2 6p7s\ ^3P_1$ level.

4. ASTRONOMICAL DATA

The stellar spectra were obtained as part of the GHRS GTO programs of D. S. Leckrone (program GTO_6245) and J. C. Brandt (program GTO_6275). All observations utilized the echelle A mode of the GHRS and the Small Science Aperture (SSA), thus maximizing the spectral resolution attainable. Observation rationale and data reduction procedures for χ Lupi spectra have previously been discussed by Wahlgren et al. (1995). All of the χ Lupi high-resolution GHRS spectra have been presented by Brandt et al. (1999), along with further details of the observations and data reduction. A scientific summary of the project, including a listing of the abundance results to date, has been presented by Leckrone et al. (1999). Data reduction for HR 7775 spectra followed the same procedures as that for χ Lupi. All observations were obtained after the *HST* First Servicing Mission, in the presence of the COSTAR instrument. An overview of the GHRS HR 7775 ultraviolet data will be provided in a forthcoming paper.

5. ABUNDANCE ANALYSES

5.1. *General Comments*

The bismuth abundances were investigated by application of a synthetic spectrum technique, whereby the observed spectra are fitted with spectra computed using the SYNTHE (Kurucz 1993) program. We have previously employed this technique as a means of aiding in line identification, elemental abundance determination, and investigation of heavy-element isotope mixtures in the analysis of χ Lupi GHRS spectra. The most recent works in this series are those for Sr and Y (Brage et al. 1998b), Zr (Sikström et al. 1999), Pt (Kalus et al. 1998), and Hg (Proffitt et al. 1999). The atomic line data, including the semiempirical line broadening constants, are from the compilation of Kurucz (1993), with limited alterations required to correct obvious inconsistencies between the observational and calculated spectra in the vicinity of the bismuth lines, as well as the new laboratory data presented in this paper. Casual inspection of the figures presented underscores the problems inherent in the use of existing line lists, particularly at vacuum ultraviolet wavelengths: an insufficient number of lines, inaccuracy of the wavelengths, and oscillator strength discrepancies. The elemental abundances for a majority of elements have been determined consistently for both stars (χ Lupi, Wahlgren, Adelman, & Robinson 1994a; HR 7775, Wahlgren et al. 2000), and it is unlikely that incorrect abundances are the cause of opacity excesses or deficiencies. Exceptions to this may arise from physical processes such as non-LTE and diffusion, in particular for lines not arising from the majority ion. Identical line lists were used for both stars when computing the spectra presented in this study.

Comparisons of the observed and calculated spectra are plotted on a normalized scale as determined by a synthetic spectrum technique (Wahlgren 1996). For the spectra containing the Bi III feature it was not possible to normalize the spectrum in this same manner. The nature of the spectrum, in terms of higher line density and missing line opacity in the calculation, rendered this technique more uncertain than expected. Thus, local normalization was accomplished by synthetic spectrum fitting of iron group element lines and by evaluating the residual flux in the spectrum high points as a fraction of the line-free continuum level. In this manner a flux scale factor was obtained for the location of the bismuth line that would simulate a normalized spectrum.

We began the bismuth analysis by study of the star χ Lupi. Elemental abundance analyses of this star and HR 7775 have shown them to be remarkably similar, with the glaring exception of strong bismuth lines in the spectrum of HR 7775. A second difference is the binary nature of χ Lupi, which allows for observable lines from the companion star. At VUV wavelengths saturated lines from the companion will attain no more than a 10% depth from the continuum level. HR 7775 is part of a multiple-star system, which includes the bright star HR 7776 (located at a distance of 205″ from HR 7775) and a close companion. The latter was observed by the *Hipparcos* astrometric satellite to be fainter by 3 mag and to lie at a distance of 0.″68 from HR 7775. This separation places the companion well outside the 0.″25

× 0″.25 SSA of the GHRS when centered on HR 7775, and we thus treat the spectrum of HR 7775 to be that of a single star. However, we also realize that since the orbit of the faint companion is unknown, so is its location with respect to the GHRS aperture at the time of the observations.

These exceptions notwithstanding, the spectra of these two HgMn stars are very similar, and owing to the great breadth of the bismuth lines arising from hfs, a study of the line blending is best accomplished from the spectrum of χ Lupi, for which the bismuth lines are weak. Unfortunately, the complexity and richness of the spectrum in the vicinity of 1400 Å does not allow for an unequivocal determination of the bismuth abundance for either star.

In the following sections we discuss lines of Bi II and Bi III, which we were able to identify in our GHRS spectra and model. The search for lines from the Bi I spectrum was hampered by line blending and the paucity of strong Bi I lines in our data sets. None of the strong lines listed in Table 1 are located in our HR 7775 data, while only two such lines (λ_{vac} = 2062.293 and 2277.261 Å) could be investigated in our more extensive χ Lupi data. Neither line has been considered in the synthetic spectrum calculations presented in the χ Lupi GHRS spectral atlas (Brandt et al. 1999), where it can be seen that identified features can account for the observed absorption at these wavelengths. As a test of the existence of observable Bi I lines, synthetic spectra were calculated for the solar abundance and a 5.0 dex enhancement for the Bi I λ2062.293 line using $gf = 0.378$, as determined from the transition probability listed by Wiese & Martin (1980). A very small difference in the blended feature profile resulted from this large enhancement level, indicating that Bi I lines in the χ Lupi spectrum would not be noticeable if the bismuth abundance is that indicated by the lines of Bi II and Bi III, and that for the bismuth enhancement determined for HR 7775 the severe line blending will prevent accurate abundance work unless a statistical approach is taken. An interesting aside pertains to the improvement of Bi I wavelengths over previous work. The air wavelength of the ground state 2062.293 Å line is determined to be λ_{air} = 2061.633 Å using the formula for the index of refraction of air by Edlén (1966). The air wavelength for this line, as listed by Moore (1962), is 2061.73 Å. This 0.1 Å difference may reflect the difficulty in measuring and presenting the wide nature of the hfs for this line. In the case of the χ Lupi GHRS spectral atlas the older wavelength would appear to correspond to an unmodeled feature in the spectrum, which was attributed to a line of Pt II by Brandt et al. (1999).

5.2. *Bismuth in χ Lupi*

Bi II *λ1436*.—The three hfs components are amply separated in wavelength to be resolved from each other in the GHRS observation. The positions of these components are detectable in Figure 3, which plots the computed spectrum for four bismuth abundance enhancements: [Bi/H] = $\log (N_{Bi}/N_H)_{Star} - \log (N_{Bi}/N_H)_{Sun}$ = 0.0 (solar), 1.4, 1.6, and 1.8. (The solar system [meteoritic] bismuth abundance by number is $\log N_{Bi} = 0.71$ on a scale where $\log N_H = 12.00$; Anders & Grevesse 1989). The features are quite sensitive to the bismuth abundance over this range. An upper limit abundance from the Bi II λ1436 line is approximately [Bi/H] = 1.6 dex. This enhancement is smaller than that obtained by an earlier study (Wahlgren et al. 1994b) from a lower resolution, first-order grating, GHRS observation of the Bi II λ1902 feature. Despite the uncertainties in line blending that exist, we cannot exclude the possibility that different abundances are extracted from lines of different excitation levels and ionization stages.

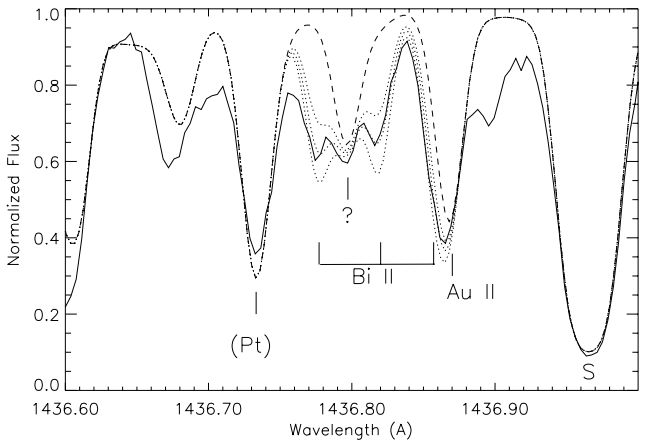

FIG. 3.—Bi II λ1436 in χ Lupi. The GHRS observation (Z2MB010I, R = 86,000; *solid line*) is compared with the synthetic spectrum for the cases of solar bismuth abundance (*dashed line*) and enhancements of the bismuth abundance by [Bi/H] = 1.4, 1.6, and 1.8 dex (*dotted lines*). The locations of the three hfs components are indicated. Other lines of note arise from Pt (unclassified line), Au II, and S I. The fictitious line introduced in the synthetic spectrum is denoted by a question mark.

The absorption feature central to the two shorter wavelength Bi II hfs components remains unidentified. Current line lists preclude this feature from being a very heavy element (Pt, Au, Hg, Tl) or singly ionized iron group elements. To treat this absorption, we have introduced a fictitious line at the wavelength 1436.797 Å. When this is done, the entire extended feature is reasonably fitted, although we cannot be certain as to the uniqueness of this treatment. If the abundance of bismuth is less than [Bi/H] = 1.5 dex, then the single fictitious line model would have to be replaced with a more complicated structure of multiple lines.

Other atomic species in this spectral interval are also of note. The strong line S I λ1436.967, originating from the ground term, required a decrease in the sulfur abundance of 0.5 dex, to $\log N_S = 6.7$, relative to the optical region abundance found from two lines of S II (Wahlgren et al. 1995). This abundance difference may be an effect of non-LTE processes operating in the upper atmospheric levels. Similar discrepancies between abundances derived from ground versus higher terms have been noted at optical wavelengths for lines of Mg II, Sr II, Hg II, and O I in HR 7775 (Wahlgren et al. 2000). This line also serves to set the absolute wavelength scale in this region for both χ Lupi and HR 7775. The heavy-element lines Au II λλ1436.6086, 1436.8681 and Pt λ1436.7340 contribute the majority of absorption observed at these wavelengths in the Figure 3 computed spectrum features. The wavelength and oscillator strength data for the Au II lines are from Rosberg & Wyart (1997), while the wavelength of the unclassified Pt line is from Reader et al. (1990). We have modeled this line as Pt II with an oscillator strength given by $\log gf = -0.6$ to account for absorption of this feature in the Bi II line wing. Abundances for Au and Pt in χ Lupi have been taken from Wahlgren et al. (1995).

Bi II *λ1902*.—The analysis of this line in χ Lupi has been presented by Wahlgren et al. (1994b). Since that study, we have revised the total *gf*-value of the transition from 0.600

to 0.725. This change has a small effect upon the previous result, that of lowering the upper limit to the abundance of bismuth from this line by 0.1 dex to [Bi/H] = 2.0 dex. We present the revised oscillator strengths for the individual hfs components in Table 11.

Bi III *λ1423*.—The four-component hfs pattern of this line is also well spaced for detection at the observation spectral resolution. Line blending is a concern for the two inner components, leaving the two outer components to provide a more sensitive indication of abundance for small levels of bismuth enhancement such as that displayed by χ Lupi. The second hfs component (λ1423.3565) is blended with two stronger lines of Fe II (λλ1423.351, 1423.334) and an unknown contributor(s). Component three (λ1423.4806) is affected by a blend with lines of Fe II (λ1423.489), Mn II (λ1423.487), and Co II (λ1423.499) and a strong unknown line near 1423.46 Å. Figure 4 depicts the absorption of these lines after having the oscillator strength for the Fe II line arbitrarily reduced from log $gf = -2.271$ to -2.771 in order not to violate the observed line profile. The absolute wavelength scale has been set by the well-fitted line Fe II λ1423.691, while the equally well-fitted line of comparable strength Cr II λ1423.807 was used in this capacity for HR 7775.

The contributions of the less blended components appear to be smaller than predicted by the LTE synthetic spectrum calculated assuming the 1.6 dex enhancement found from our fit to the Bi II λ1436 line. Any increased line depth resulting from an enhancement of bismuth is rivaled by the amplitude of noise artifacts. We must therefore conclude that this Bi III line does not support a bismuth enhancement of even as much as 1 dex. Abundance enhancements at a level of 1.6 dex, as derived from the Bi II lines, would produce obvious Bi III absorption features in Figure 4. This suggests an ionization anomaly of 0.6 dex, and perhaps larger depending upon observed noise levels and the accuracy of the oscillator strengths.

5.3. *Bismuth in HR 7775*

Bi II *λ1436*.—Choice of the best fit is contingent upon several assumptions. Figure 5 compares the observed spectrum with synthetic spectra calculated for bismuth enhancements [Bi/H] = 0.0 (solar), 4.7, and 4.8 dex. The spectra have been flux normalized using the entire observation, which extends over 8 Å, and synthesized spectra. High points at the level of the synthesized continuum and well-fitted lines do exist in this region, unlike the region at 1423 Å. The wavelengths of the three Bi II components, known to milliangstrom accuracy, agree well with the S I wavelength calibration. It is also clear that 4.8 is entirely consistent with the observed line profile while 4.9 would violate the line profile to some degree. The outstanding issue remains the true nature of the unknown blending, which was modeled for χ Lupi by a fictitious λ1436.797 line, and which is modeled here in a similar fashion. We can only assume that the unknown line is likely to behave in a similar manner for both stars since their spectra are so similar. Nevertheless, the wavelength of this line can be seen in Figure 5 to affect the abundance level chosen for bismuth. The bismuth abundance may also be artificially high by exclusion of absorptions from the interstellar medium, which may have a greater influence in HR 7775 than in χ Lupi as a result of the former being more distant. To account for line blending by lines of platinum and gold, we have determined their abundances of (log $N_{Pt} = 6.5$, log $N_{Au} = 4.8$) via synthetic spectrum fitting of GHRS spectra using atomic line data for the strong lines Pt II λ2144 (Kalus et al. 1997) and Au II λ1740 (Wahlgren et al. 1995).

Bi II *λ1902*.—This feature was analyzed using the hfs component wavelengths presented by Wahlgren et al. (1994b) and the revised *gf*-values listed in Table 11. The red side of the feature profile is affected by blending with the autoionization line of Si II, which has not been included in our modeling. Figure 6 presents the fit to the observed line profile for the three bismuth abundances [Bi/H] = 0.0 (solar), 4.8, and 5.3 dex. The feature appears to be best fitted for an abundance of 5.3. The fit to the blue side of the feature can be altered by the uncertainty of the oscillator strength for the unclassified Pt λ1902.26 line. The fit to the redward side is influenced by uncertainties in the *f*-values for the Fe II lines (λλ1902.412, 1902.418, 1902.438) and the shape and extent of the unmodeled absorption related to the Si II line. The uneven nature of the Bi II feature trough

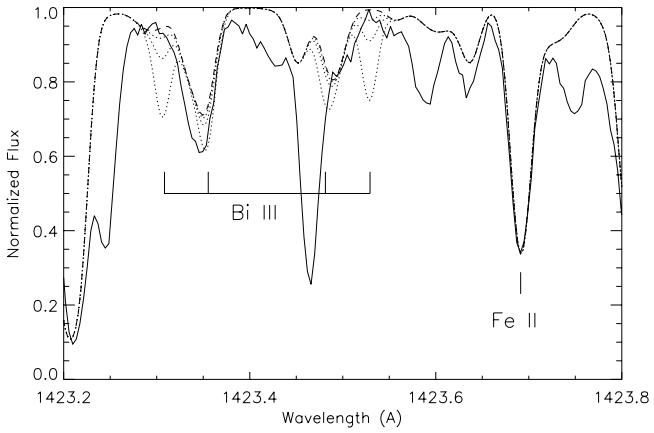

FIG. 4.—Bi III λ1423 in χ Lupi. The GHRS observation (Z3650308, $R = 82{,}000$; *solid line*) is compared with the synthetic spectrum for the cases of solar bismuth abundance (*dashed line*) and enhancements of the bismuth abundance by [Bi/H] = 1.0, 1.5, and 2.1 dex (*dotted lines*). The four hfs components are indicated. The labeled Fe II λ1423.691 line has been used to set the absolute wavelength scale.

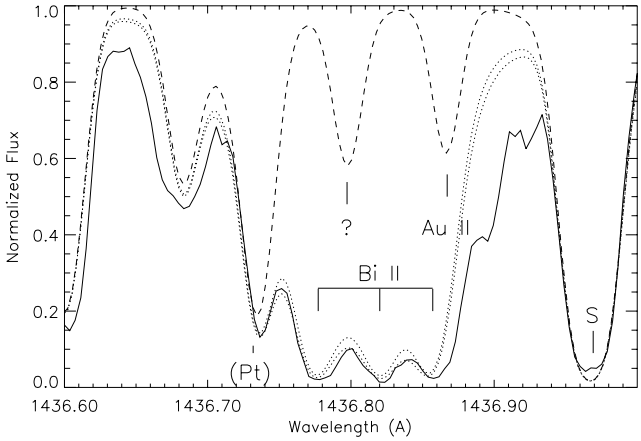

FIG. 5.—Bi II λ1436 in HR 7775. The GHRS observation (Z32M0107, $R = 86{,}000$; *solid line*) is compared with the synthetic spectrum for the cases of solar bismuth abundance (*dashed line*) and enhancements of the bismuth abundance by [Bi/H] = 4.7 and 4.8 dex (*dotted lines*). The locations of the three hfs components are labeled.

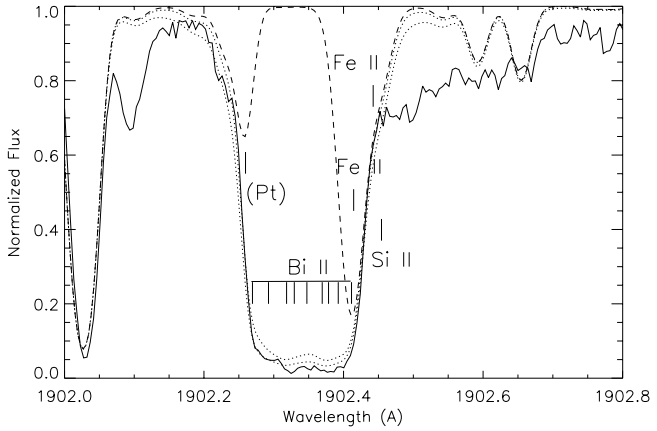

FIG. 6.—Bi II λ1902 in HR 7775. The GHRS observation (Z32M010A, $R = 94{,}000$; *solid line*) is compared with the synthetic spectrum for the cases of solar bismuth abundance (*dashed line*) and enhancements of the bismuth abundance by [Bi/H] = 4.8 and 5.3 dex (*dotted lines*). The locations of the hfs components for this transition are denoted, as well as the most obvious blends from an unclassified Pt line, Fe I, Fe II, and the location of the Si II λ1902.45 autoionization feature.

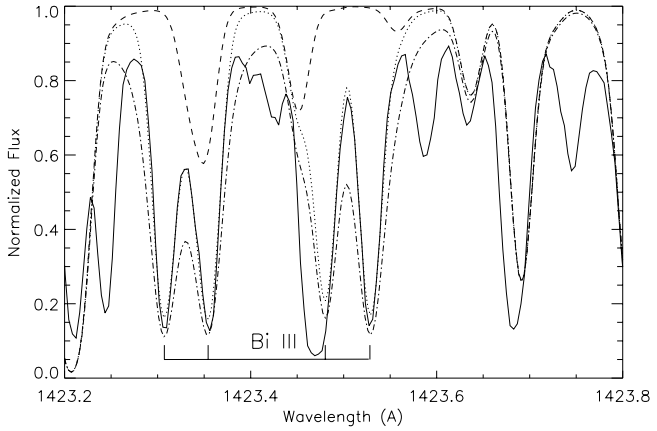

FIG. 7.—Bi III λ1423 in HR 7775. The GHRS observation (Z3650308, $R = 82{,}000$; *solid line*) is compared with synthetic spectra for the cases of solar system bismuth abundance (*dashed line*) and an enhancement of [Bi/H] = 5.0 dex in which the radiative and Stark damping constants are classical (*dot-dashed line*) and altered (*dotted lines*) values (described in text). Several features in the vicinity of the Bi lines remain unidentified and would lead to an overestimate of the Bi abundance if observed at lower (*IUE*) spectral resolution.

may attest to absorption by unmodeled features, as well as to noise in the data. Therefore, our best-fit abundance should be interpreted as an upper limit.

Bi III *λ1423*.—The four hyperfine components are all observed. Blending with lines noted for the χ Lupi analysis is now aggravated by the increased strength of the latter. The cobalt oscillator strength was reduced from $\log gf = -2.221$ to -2.600, in conjunction with use of the solar cobalt abundance, in order that the Co II λ1423.499 line does not violate the observed line profile for the case of solar bismuth abundance. The unknown line at 1423.46 Å in the spectrum of χ Lupi is also present in HR 7775 at a comparable strength.

In addition to blending with unknown lines, the fit is complicated by uncertain damping constants for the radiative and Stark line broadening mechanisms. Neither experimental nor calculated damping constants were found for this transition, and we began the analysis by employing the standard formalisms used by Kurucz (1993). For a bismuth abundance enhancement similar to that derived from the Bi II λ1902 line it is clear that the line widths are computed too wide. A reduction in abundance serves to fit better the line wings at the expense of the line core depth and introduces an artificial conflict in ionization balance between Bi^+ and Bi^{++}. By using the radiative transition probabilities from our calculations, the radiative damping constant is reduced from the classical value of $\log \gamma_{rad} = 9.04$ to 8.05. This result is not unexpected since the radiative decay lifetime for intercombination lines can be longer than for normal allowed transitions. This reduction leads to the discrepancy between the observed and computed line profiles to be reduced by half. Although a further reduction of $\log \gamma_{rad}$, to approximately 7.0, could better match the line profile, the resulting lifetime would not agree with the calculations, and we chose not to alter the value derived from the calculation. Instead, to account for the remainder of the line broadening discrepancy, the Stark damping constant was reduced by 1 order of magnitude, from $\log \gamma_S = -5.85$ to -6.85. Figure 7 reflects the fits when using the original damping constants and the reductions in $\log \gamma_{rad}$ and $\log \gamma_S$ by 1 order of magnitude. With these revised damping constants the abundance of bismuth is determined to be enhanced by 5.3 dex, which is a similar value to that derived from Bi II λ1902. This apparent agreement in abundance between the ions Bi^+ and Bi^{++} may be strictly fortuitous in light of our LTE analysis, and it may later be shown that the Bi III ground state transition is more affected by non-LTE or diffusion than Bi II λ1902. The need for non-LTE physics may also be indicated by the 0.5 dex abundance difference between the ground state transition Bi II λ1436 and the Bi II λ1902 line.

6. CONCLUSIONS

The abundance of bismuth has been investigated in the cool HgMn stars χ Lupi and HR 7775 by fitting observed spectral line profiles obtained with the *HST*/GHRS with synthetic spectra computed under conditions of LTE model atmospheres. A summary of our results is presented in Table 12. Of critical importance to the analysis are accurate wavelengths for all hfs components for the transitions studied and a detailed knowledge of line blending. We have addressed the first point by laboratory measurements acquired at an accuracy of 1–2 mÅ for strong lines of the neutral state and the first two ions of bismuth. Oscillator strengths and hyperfine splitting for select lines of Bi II and Bi III are presented from calculations.

TABLE 12

BISMUTH ABUNDANCES[a] IN χ LUPI AND HR 7775

Wavelength (Å)	Ion	χ Lupi	HR 7775
1436.....	Bi II	<2.3	5.5
1902.....	Bi II	<2.7	6.0
1423.....	Bi III	<1.7	6.0

[a] $\log N_{Bi}$ includes solar system value of 0.7 dex.

For χ Lupi the enhancement of bismuth above solar levels is constrained to be less than 1.6 dex from Bi II λ1436 and 2.0 dex from Bi II λ1902. Uncertainties in the treatment of line blending and oscillator strengths alone may account for the difference in these upper limits. The result for Bi^{+} is in contrast with that for Bi^{++}, for which no absorption is apparent from the Bi III λ1423 resonance line. Uncertainties in the observation noise level and continuum placement place a loose upper limit on the bismuth abundance to be at an enhancement level of 1 dex. No absorption from Bi III is apparent, and an ionization anomaly between the resonance lines of Bi II and Bi III may therefore be as high as 1.5 dex as a result of data noise.

In contrast to χ Lupi, the spectrum of HR 7775 presents saturated lines for Bi II $\lambda\lambda$1436 and 1902. A consistent abundance can be derived from these two lines within the uncertainties of line blending and the oscillator strengths. The bismuth enhancement is found to be 5 orders of magnitude above the solar system value. A similar abundance enhancement is found from the Bi III λ1423 intercombination line. Therefore, an ionization anomaly is not suggested for HR 7775 as it is for χ Lupi. However, caution is required in this interpretation because of the uncertain nature of the line damping constants and the need for abundance calculations to be made under non-LTE assumptions. The bismuth enhancement level that we have determined is approximately 1 dex less than that determined by Jacobs & Dworetsky (1982) from *IUE* spectra of this star. Our treatment of the hfs components and line blending, the latter resulting from the vastly different spectral resolutions of the *IUE* and *HST*/GHRS data, is likely to account for this difference.

The results of the abundance analysis confirm previous general knowledge of bismuth in χ Lupi and HR 7775 and provide a more detailed account of the line blending in the vicinity of the resonance lines Bi II λ1436 and Bi III λ1423. The atomic line data can now serve as templates for a more systematic search for bismuth absorption in other chemically peculiar stars. It is also necessary to investigate additional lines from these ions in the spectrum of HR 7775 to substantiate suspicions regarding a bismuth ionization anomaly.

The determination of abundance enhancements in HR 7775 from UV transitions for platinum, [Pt/H] = 4.7 dex, and gold, [Au/H] = 3.8 dex, substantiates similar values from optical region data (Wahlgren et al. 2000). The enhanced abundance peak for the elements Pt, Au, Hg, and Tl is very similar for χ Lupi and HR 7775, yet bismuth provides a markedly different result that requires an investment in theoretical modeling in terms of non-LTE and diffusion processes. However, conducting useful numerical experiments in non-LTE requires additional atomic data. In particular, estimates of photoionization cross sections for the lower levels of Bi I and Bi II lines, in addition to estimates of transition probabilities for a large number of lines, will allow complex model ions to be constructed.

An investment in acquiring atomic data for bismuth may prove to be particularly rewarding for understanding the CP star phenomenon. Among the HgMn stars the elements mercury and manganese are well known for their line strength enhancements. The spectral behavior of other heavy elements, platinum and gold, for example, also appears linked to that of mercury. Such is apparently not the case for bismuth, as it is only HR 7775 that has been found to display strong bismuth spectral lines among HgMn stars. Under further scrutiny other HgMn stars, such as χ Lupi, will show small enhancements of bismuth lines. Therefore, strong enhancement of bismuth lines may represent a brief period in the lifetime of a CP star and may thus provide valuable insight into atmospheric structure and dynamics and stellar age. As such bismuth may reveal itself to be a sensitive temporal discriminant of the CP star phenomenon.

This research was supported in part by NASA grant NAGW-2908. G. M. W. gratefully acknowledges financial support received from the Swedish Royal Academy of Sciences. Work at NIST was supported in part by the US National Aeronautics and Space Administration.

REFERENCES

Anders, E., & Grevesse, N. 1989, Geochim. Cosmochim. Acta, 53, 197
Biéron, J. R., Marcinek, R., & Migdalek, J. 1991, J. Phys. B, 24, 31
Brage, T., Leckrone, D. S., & Froese Fischer, C. 1996, Phys. Rev. A, 53, 192
Brage, T., Proffitt, C. R., & Leckrone, D. S. 1998a, ApJ, 513, 524
———. 1999, J. Phys. B, 32, 1
Brage, T., Wahlgren, G. M., Johansson, S. G., Leckrone, D. S., & Proffitt, C. R. 1998b, ApJ, 496, 1051
Brandt, J. C., et al. 1999, AJ, 117, 1505
Clearman, H. E. 1952, J. Opt. Soc. Am., 42, 373
Cowley, C. R. 1987, Observatory, 107, 188
Crawford, M. F., & McLay, A. B. 1934, Proc. R. Soc. London A, 143, 540
Curtis, L. J., Ellis, D. G., Matulioniene, R., & Brage, T. 1997, Phys. Scr., 56, 240
Edlén, B. 1966, Metrologia, 2, 71
George, S., Munsee, J. H., & Vergès, J. 1985, J. Opt. Soc. Am. B, 2, 1258
Grant, I. P. 1988, Methods Comput. Chem., 2, 1
Grant, I. P., McKenzie, B. J., Norrington, P. H., Mayers, D. F., & Pyper, N. C. 1980, Comput. Phys. Commun., 21, 207
Henderson, M., Curtis, L. J., Ellis, D. G., Irving, R. E., & Wahlgren, G. M. 1996, ApJ, 473, 565
Jacobs, J. M., & Dworetsky, M. M. 1982, Nature, 299, 535
Jönsson, P., Parpia, F. A., & Froese Fischer, C. 1996, Comput. Phys. Commun., 96, 301
Kalus, G., Johansson, S., Wahlgren, G. M., Leckrone, D. S., Thorne, A. P., & Brandt, J. C. 1998, ApJ, 494, 792
Kurucz, R. L. 1993, Kurucz CD-ROM 18, SYNTHE Synthesis Programs and Line Data (Cambridge: SAO)
Leckrone, D. S., Johansson, S., Kalus, G., Wahlgren, G. M., Brage, T., & Proffitt, C. R. 1996, ApJ, 462, 937
Leckrone, D. S., Johansson, S. G., Wahlgren, G. M., Proffitt, C. R., & Brage, T. 1998, in ASP Conf. Ser. 143, The Scientific Impact of the Goddard High Resolution Spectrograph, ed. J. C. Brandt, T. B. Ake, III, & C. C. Petersen (San Francisco: ASP), 135
Leckrone, D. S., Proffitt, C. R., Wahlgren, G. M., Johansson, S. G., & Brage, T. 1999, AJ, 117, 1454
Mathews, C. W., Ginter, M. L., Ginter, D. S., & Brown, C. M. 1989, J. Opt. Soc. Am. B, 2, 1627
McKenzie, B. J., Grant, I. P., & Norrington, P. H. 1980, Comput. Phys. Commun., 21, 233
Michaud, G. 1970, ApJ, 160, 641
Moore, C. E. 1958, Atomic Energy Levels, Vol. III, Natl. Bur. Std. Circ. 467 (Washington DC: US Gov. Printing Office)
———. 1962, An Ultraviolet Multiplet Table, Natl. Bur. Std. Circ. 488 (Washington DC: US Gov. Printing Office)
Mrozowski, S. 1942, Phys. Rev., 62, 526
Parpia, F., Froese Fischer, C., & Grant, I. P. 1996, Comput. Phys. Commun., 94, 249
Proffitt, C. R., Brage, T., Leckrone, D. S., Wahlgren, G. M., Brandt, J. C., Sansonetti, C. J., Reader, J., & Johansson, S. G. 1999, ApJ, 512, 942
Reader, J., Acquista, N., Sansonetti, C. J., & Sansonetti, J. E. 1990, ApJS, 72, 831
Rosberg, M., & Wyart, J.-F. 1997, Phys. Scr., 55, 690
Ross, C. B. 1970, Los Alamos Scientific Laboratory Rep. 4498 (Springfield: National Technical Information Service)
Sansonetti, J. E., Reader, J., Sansonetti, C. J., & Acquista, N. 1992, J. Res. NIST, 97, 1
Seaton, M. J. 1997, MNRAS, 289, 700
———. 1999, MNRAS, 307, 1008

Sikström, C. M., Lundberg, H., Wahlgren, G. M., Li, Z. S., Lyngå, C., Johansson, S., & Leckrone, D. S. 1999, A&A, 343, 297
Wahlgren, G. M. 1996, in ASP Conf. Ser. 108, Model Atmospheres and Spectrum Synthesis, ed. S. J. Adelman, F. Kupka, & W. W. Wiese (San Francisco: ASP), 240
Wahlgren, G. M., Adelman, S. J., & Robinson, R. D. 1994a, ApJ, 434, 349
Wahlgren, G. M., Dolk, L., Kalus, G., Johansson, S., Litzén, U., & Leckrone, D. S. 2000, ApJ, 539, 908
Wahlgren, G. M., et al. 1994b, ApJ, 435, L67
Wahlgren, G. M., Leckrone, D. S., Johansson, S., Rosberg, M., & Brage, T. 1995, ApJ, 444, 438
Wiese, W. L., & Martin, G. A. 1980, Wavelengths and Transition Probabilities for Atoms and Atomic Ions, Part II: Transition Probabilities (Washington DC: US Gov. Printing Office)